Modeling and Experiment Design for Identification of Wear in a Robot Joint under Load and Temperature Uncertainties based on Friction Data

André Carvalho Bittencourt and Patrik Axelsson

***Abstract*—The effects of wear to friction are studied based on constant-speed friction data collected from dedicated experiments during accelerated wear tests. It is shown how the effects of temperature and load uncertainties produce larger changes to friction than those caused by wear, motivating the consideration of these effects. Based on empirical observations, an extended friction model is proposed to describe the effects of speed, load, temperature and wear. Assuming availability of such model and constant-speed friction data, a maximum likelihood wear estimator is proposed. The performance of the wear estimator under load and temperature uncertainties is found by means of simulations and verified under three case studies based on real data. Practical issues related to experiment length are considered based on an optimal selection of speed points to collect friction data, improving the achievable performance bound for any unbiased wear estimator. As it is shown, reliable wear estimates can be achieved even under load and temperature uncertainties, making condition based maintenance of industrial robots possible.**

***Index Terms*—industrial robotics, wear, friction, identification, condition monitoring**

I. INTRODUCTION

INDUSTRIAL robots are used as a key factor to improve productivity, quality and safety in automated manufacturing. Robot installations are many times of crucial importance in the processes they are used and an unexpected robot stop or malfunction may lead to production and economical losses. Increased safety, reliability, availability and maintainability (SRAM) are therefore critical for industrial robots. Preventive scheduled maintenance is a common approach to guarantee the requirements on SRAM in the manufacturing industry. Such scheduling is often determined from the estimated lifespan of robot components, with considerable margins. Because preventive maintenance is not determined by the actual robot condition, unnecessary maintenance actions might take place.

In the current scenario, maintainability of industrial robots can be greatly improved with the use of methods to determine its condition, allowing for condition based maintenance (CBM). With focus on service, it is important that a change in condition is detected before a critical degradation takes place, so that timely maintenance actions can take place. Wear in a robot joint may lead to a degradation of performance and to an eventual failure. Because wear typically develops slowly with time and usage, it might be detectable in an early stage, making CBM possible.

Wear can be defined as "the progressive loss of material from the operating surface of a body occurring as a result of relative motion at its surface" [1]. The need for relative motion between surfaces implies that the wear mechanisms are related to *mechanical action* between surfaces. This is an important distinction to other processes with a similar outcome and very different nature, e.g. corrosion [2]. Wear is naturally related to friction since friction can be defined as the tangential reaction force between two surfaces in contact. Friction always opposes motion, dissipating kinetic energy. A part of the work produced by friction appears as heat transfer, vibrations and acoustic emissions. Other outcomes of friction are plastic deformation, adhesion and fracture which relate to wear.

The accumulated wear in a tribosystem may lead to variations in friction [3], [4]. Alternatives for wear monitoring are thus possible provided it is applicable to *observe friction* and the relation between *friction and wear* is known. Monitoring friction to infer about wear is however challenging since friction is significantly affected by other factors than wear such as temperature and load. The effects of temperature are specially difficult since temperature is not measured in typical robot applications. These co-effects should nevertheless be considered when verifying the reliability of a solution.

In the literature, little can be found about wear estimation for industrial robots. This may be attributed to the lack of wear models available and the high costs and time required to perform wear experiments. There are related approaches used for *fault detection*, where the objective is to decide whether a change from nominal is present. Faults are typically considered as actuator malfunctions, modeled as changes in the output torque signals or in the parameters of a robot model. This includes the case of *friction changes*, which is important since they can relate to wear.

The use of *nonlinear observers*, as presented in [5]–[10], is important to support control law reconfiguration and fault detection. In [11], an observer is used to estimate friction torques in a rotating machine; the presence of a friction change is detected based on a multiple hypotheses test where each hypothesis is associated to a known friction model. In [12], *energy balance* equations are monitored for fault detection and isolation; the framework is illustrated with a simulation study of a robot manipulator with faults in dissipative components (e.g. friction changes) and energy-storing components (e.g.

The authors are with the Department of Electrical Engineering, Linköping University, Linköping, Sweden. {andrecb, axelsson}@isy.liu.se

This work was supported by ABB and the Vinnova Industry Excellence Center LINK-SIC at Linköping University.

load changes). Because the energy balance is also affected by disturbances, knowledge of these effects to the system's energy can be used to achieve robustness; some approaches are discussed in [12], see also [13].

The *estimation of friction parameters* in a robot model from measured data is a natural approach because of the physical interpretation of these parameters. In [14], estimates of the Coulomb and viscous friction parameters are compared to confidence values of their nominal behavior. In the experimental study presented, these parameters could indicate some of the faults but could not readily distinguish between them; e.g. the increase of joint temperature had a similar effect as a fault in the drive-chain. As illustrated here, the effects of wear and temperature affect friction in a similar manner and the simple friction model used in [14] did not consider this. The effects of temperature to friction were considered in [15], where estimates of the viscous friction parameter are used to monitor the lubricant health in a mechanical transmission. The lubricant temperature is estimated based on a Kalman filter using environment temperature measurements and a heat transfer model. A similar approach but based on an observer of the viscous friction torque is also presented in [16] with simulation studies for a robot joint.

In this paper, a wear estimator is proposed based on a known friction model and constant-speed friction data which are achieved through *dedicated experiments*, in an off-line manner. A solution based on dedicated experiments will decrease the robot availability which is undesirable from the perspective of a robot user. The trade-off between experiment length and the estimator accuracy is therefore important and is studied in detail. The **main contributions** leading to the proposed solution are listed

- first, the effects of wear to friction are modeled based on empirical observations;
- an extended friction model is proposed and identified to describe the effects of speed, temperature, load and wear;
- with a known friction model, maximum likelihood wear estimators are proposed;
- experiment design is considered based on the achievable performance for any unbiased wear estimator;
- the estimator is validated through simulations and case studies based on real data.

These results are presented through Secs. II-C to V. Secs. II-A and II-B review earlier results presented in [17] which are used in this paper; namely, an experiment routine used to provide constant-speed friction data and a friction model to describe the nominal behavior of friction, i.e. under no considerable presence of wear. The conclusions and proposals for further research are presented in Sec. VI. The studies presented in the paper are based on observed friction in joint 2 of ABB IRB 6620 industrial robots. Joint 2 is chosen for the study as it endures great stress variations for the type of robot considered. The joint is equipped with a rotary vector type of gearbox which is commonly found in industrial robots of similar sizes.

A preliminary version of a wear estimation approach based on constant-speed friction data was presented in [4] where the wear model was first presented and a prediction-error wear estimator was suggested and verified. Here, wear estimators are suggested based on a statistical framework, with a more in-depth study of experiment design, achievable performance and verification studies.

II. STEADY-STATE FRICTION IN A ROBOT JOINT

Friction is a dynamic phenomenon. At a contact level, the surfaces' asperities can be compared to (very stiff) bristles in a brush, each of which can be seen as a body with its own dynamics connected by the same bulk [18], [19]. Because the internal friction states are not measurable, it is common to study friction in steady-state, when friction presents a static behavior. Experimental data show that under *constant speed*, the friction in a robot joint can be described by a static function, see e.g. [17].

The simplified behavior of steady-state friction[1] makes it easier to be modeled and to identify the sources of changes, e.g. caused by wear or temperature. A shortcoming is that constant-speed data are not readily available from a robot normal operation. This type of data can however be collected based on the experimental procedure described in [17]. Data collected from such an experiment will be used as input to the wear estimators suggested here and the procedure is briefly described in Sec. II-A.

Friction in a robot joint is affected by many factors. Using constant-velocity friction data, the behavior of steady-state friction is studied in detail in [17] where a static nonlinear model was suggested to describe the effects of speed, temperature and load. This model is reviewed in Sec. II-B and extended in Secs. II-C and II-D to include a description of observed changes caused by wear.

A. A Procedure to Estimate Friction at a Fixed Speed Level

A simple procedure is suggested in [4], [17] for the estimation of constant-speed friction data which is revised here. A manipulator is a multivariable, nonlinear system that can be described in a general manner through the rigid multi-body dynamic model

$$M(\varphi)\ddot{\varphi} + C(\varphi, \dot{\varphi}) + \tau_g(\varphi) + \tau_f = \tau \tag{1}$$

where φ is the motor position, $M(\varphi)$ is the inertia matrix, $C(\varphi, \dot{\varphi})$ relates to Coriolis and centrifugal terms, $\tau_g(\varphi)$ are the gravity-induced joint torques and τ_f contains the joint friction components. The system is controlled by the input torque, τ, applied by the joint motor (in the experiments the torque reference from the servo was measured)[2]. For single joint movements (so that centrifugal forces are zero at that joint) and under constant speed (so that inertial torques are zero), the

[1] In this paper, the term steady-state friction is used as a synonym of the friction observed in constant-speed conditions.

[2] It is known that using the torque reference from the controller as a measure of the joint torque might not always hold. The torque controller for the robot considered in the studies has a steady-state error of maximum 5%. The variations are because of the temperature dependence of the torque constant of the motors.

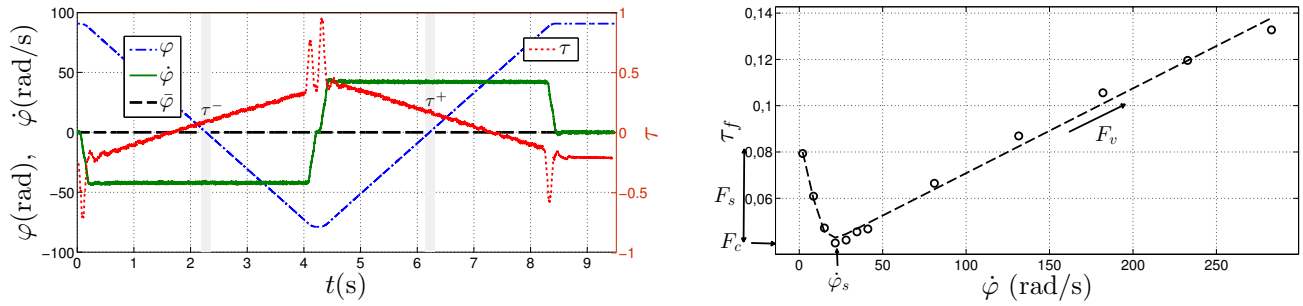

(a) Data collected for the estimation of the friction level at $\bar{\dot{\varphi}}=42$ and $\bar{\varphi}=0$. (b) Estimated friction levels (circles) and predictions based on (4).

Fig. 1. Experimental procedure for the estimation of constant-speed friction. Data are collected for single joint movements back and forth around a position $\bar{\varphi}$ for a desired speed $\bar{\dot{\varphi}}$, as shown in (a). The constant speed torque levels for the forward and backward movements, τ^+ and τ^- respectively, are segmented and used for estimation of τ_f according to (3). The procedure can be repeated for different speed levels and plotted against speed in a friction curve as shown by the circles in (b). The dashed line corresponds to predictions computed based on the model in (4) with an interpretation of the model parameters.

applied torque at the joint drives only gravity induced torques and friction, i.e.

$$\tau_g(\varphi) + \tau_f = \tau. \tag{2}$$

By considering forwards and backwards movements for a speed level $\bar{\dot{\varphi}}$ around a position $\bar{\varphi}$ (so that $\tau_g(\bar{\varphi})$ is the same in both directions), a *direction independent* estimate of friction can be achieved as

$$\tau_f = (\tau^+ - \tau^-)/2 \tag{3}$$

where τ^+ and τ^- are the resulting torques when the joint is moved forwards, respectively backwards. In the experiments, each joint is moved separately with the desired speed $\bar{\dot{\varphi}}$ in both directions around a given joint angle $\bar{\varphi}$. As an example, Fig. 1(a) shows the measured joint angle-, speed- and torque[3] data generated from such experiment in joint 2 of an ABB IRB 6620. The constant speed data are segmented around $\bar{\varphi}$ and the constant-speed friction levels are achieved based on (3). The procedure can be repeated for several $\bar{\dot{\varphi}}$'s and a *friction curve* can be drawn, which contains steady-state friction values plotted against speed, see Fig. 1(b). The average time required to execute the trajectory to estimate friction at one speed was optimized down to 2.5 s.

Friction data collected using such procedure simplifies the wear estimation problem since the experiment is performed in a controlled manner, reducing the effects of external disturbances (found, e.g., in contact applications) and it does not depend on a robot model, which may contain uncertainties. The fact that it does not account for possible direction dependencies of friction is not critical considering that wear would cause a generalized increase of friction which is captured by (3). Considering that performing experiments with the robot will reduce its availability, it is important to reduce the number of friction data required to provide accurate wear estimates. As it will be shown, the choice of which and how many speed levels where friction data are collected are *important design parameters*, affecting the quality of the wear estimates and the length of the experiments.

[3]Throughout the paper all torques are normalized to the maximum manipulation torque at low speed and are therefore displayed as dimensionless quantities. All velocity measurements have values shown in the motor side, before the reduction.

B. A Model for the Nominal behavior of Friction

The behavior of friction in a robot joint is considerably affected by other variables than wear. To allow for a reliable discrimination of wear, it is therefore important that the effects caused by these variables are well understood. A common description of a direction independent friction curve is given according to

$$\tau_f(\dot{\varphi}) = F_c + F_s e^{-\left|\frac{\dot{\varphi}}{\dot{\varphi}_s}\right|^\alpha} + F_v\dot{\varphi} \tag{4}$$

which is valid for $\dot{\varphi} > 0$ and where $F_c, F_s, F_v, \varphi_s, \alpha \geq 0$ are model parameters. The offset term F_c is known as the Coulomb parameter; $F_s e^{-\left|\frac{\dot{\varphi}}{\dot{\varphi}_s}\right|^\alpha}$ describes the decay of friction at intermediate speeds (Stribeck phenomenon) which is common in lubricated friction, and tends to zero with speed according to the Stribeck speed parameter $\dot{\varphi}_s$ and exponent α; the term $F_v\dot{\varphi}$ represents the viscous behavior of friction, increasing friction at high speeds, see Fig. 1(b). Based on a comprehensive experimental study of steady-state friction in an industrial robot joint, this model was extended in [17] to include a description of temperature and load according to

$$\tau_f^0(\dot{\varphi}, \tau_l, T) = \{F_{c,0} + F_{c,\tau_l}\tau_l\} + F_{s,\tau_l}\tau_l e^{-\left|\frac{\dot{\varphi}}{\dot{\varphi}_{s,\tau_l}}\right|^\alpha} + \tag{5a}$$

$$+ \{F_{s,0} + F_{s,T}T\} e^{-\left|\frac{\dot{\varphi}}{\{\dot{\varphi}_{s,0}+\dot{\varphi}_{s,T}T\}}\right|^\alpha} + \tag{5b}$$

$$+ \{F_{v,0} + F_{v,T} e^{\frac{-T}{T_{V0}}}\}\dot{\varphi}, \tag{5c}$$

where τ_l is the absolute value of the manipulated load torque and T is the joint temperature, the remaining variables are parameters used to model the friction behavior. The model (5) extends the parameters F_c, $F_s, \dot{\varphi}_s$ in (4) as a linear function of T and τ_l, where the exponential terms present a different behavior for τ_l and T; the viscous slope parameter F_v is extended as a nonlinear function of T. A similar description of load has also been reported for different devices in [20], [21] and an exponential behavior of viscous friction with temperature was also reported in [15].

In [17], the parameters in (5) were found for axis 2 of an ABB IRB 6620 industrial robot with the use of joint temperature measurements and an estimate of τ_l based on a robot model; the parameter values are given in Table I. Fig. 2(a) presents observed and model-based predictions of

TABLE I
IDENTIFIED PARAMETERS FOR THE MODEL (5), VALUES TAKEN FROM [17].

$F_{c,0}$	F_{c,τ_l}	$F_{s,0}$	F_{s,τ_l}	$F_{s,T}$	$F_{v,0}$	$F_{v,T}$	$\dot{\varphi}_{s,0}$	$\dot{\varphi}_{s,\tau_l}$	$\dot{\varphi}_{s,T}$	T_{Vo}	α
$3.11\,10^{-2}$	$2.34\,10^{-2}$	$-2.50\,10^{-2}$	$1.26\,10^{-1}$	$1.60\,10^{-3}$	$1.30\,10^{-4}$	$1.32\,10^{-3}$	-24.81	9.22	0.98	20.71	1.36

friction curves for high and low values of τ_l and T. Notice the effects of τ_l, which give an offset increase of the whole curve together with an exponential-like increase at speeds below 25 rad/s. The effects of T can be seen as an exponential increase at speeds below 80 rad/s and a decrease of the curve slope at higher speeds. Notice further that for such temperature and load values, there is a speed range where the effects are less pronounced, in this case around 80 rad/s.

1) Validation: As shown in [17], the model in (5) can be used to predict the behavior of steady-state friction under broad operation conditions. This model can thus be used as a description of the nominal (wear free) behavior of friction. The mean and standard deviation of the prediction error for the model in (5), denominated here as ε, were estimated based on more than 5800 steady-state friction data points collected under different speed, temperature and load conditions as $[\mu_\varepsilon, \sigma_\varepsilon] = [-9.24\,10^{-4}, 4.23\,10^{-3}]$. The same evaluation for a model based on (4), dependent only on speed, gave a mean and standard deviation for the error as $[1.09\,10^{-2}, 1.34\,10^{-2}]$ which are considerably larger.

C. A Model of the Wear effects to Friction

Monitoring a robot until a failure takes place is a costly and time consuming task and it is thus difficult to fully comprehend the effects of wear in a robot joint. An alternative is considered here based on data collected from accelerated wear tests, where the robot is run continuously under high load and stress levels for several months or years until failure. The resulting friction curves from such experiment at joint 2 of an ABB IRB 6620 robot are shown in Fig. 2(b), which were obtained under the *same load- and temperature levels*. The different speed dependency of these effects compared to those caused by temperature and load in Fig. 2(a) is an important characteristic of the problem. It shows that a careful selection of speed levels is needed to obtain an accurate determination of wear based on friction data.

Resolving for coupled effects between wear, temperature, load and other parameters would require costly long term experiments which are inviable even for accelerated tests. A simplifying assumption is taken that considers the effects of load and temperature to be *independent* from those caused by wear. Under this assumption, the effects of wear can be isolated in friction data collected under constant load and temperature conditions, such as the friction curves of Fig. 2(b). From such data, a **wear profile** quantity, $\widetilde{\tau}_f$, is defined by subtracting nominal friction data, observed before the accelerated wear tests started, τ_f^0, from the ones obtained thereafter i.e.,

$$\widetilde{\tau}_f = \tau_f - \tau_f^0. \tag{6}$$

The resulting wear profile from the accelerated wear tests in Fig. 2(b) can be seen in Fig. 3, where friction is presented

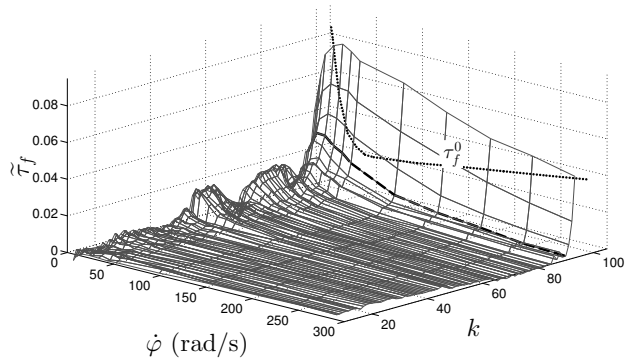

Fig. 3. Friction wear profile $\widetilde{\tau}_f$ computed from the data in Fig. 2(b) according to (6). The dotted line relates to the nominal (wear-free) friction curve τ_f^0 removed from the friction data. The dashed line indicates a wear level considered important to be detected.

along k and $\dot{\varphi}$.

As can be noticed, the effects of wear appear as an increase of friction in the low to intermediate speeds region (related to the Stribeck phenomenon), and a small decrease of the viscous friction velocity slope. Introducing w as a wear parameter, the observations support the choice of a model structure for the wear profile as

$$\widetilde{\tau}_f(\dot{\varphi}, \mathsf{w}) = F_{s,\mathsf{w}}\mathsf{w}e^{-\left|\frac{\dot{\varphi}}{\dot{\varphi}_{s,\mathsf{w}}\mathsf{w}}\right|^\alpha} + F_{v,\mathsf{w}}\,\mathsf{w}\dot{\varphi}, \tag{7}$$

where $F_{s,\mathsf{w}}$, $\dot{\varphi}_{s,\mathsf{w}}$, $F_{v,\mathsf{w}}$ and α are model parameters. Except for the offset term, the model has a similar structure as (4) with coefficients dependent on w. The variable w relates to the degree of which the wear effects appear in the observed friction and it is not a physical quantity nor can it be measured. The wear parameter w is defined by convention with values between $[0,\ 100]$, relative to a failure state, and is a dimensionless quantity.

The value $\mathsf{w} = 100$ denoting a failure state should be defined as the point where the robot fails to perform according to the requirements imposed by the application. Clearly, a failure is always present in case the robot condition leads to a robot stop. While a robot stop may be caused by a total mechanical failure of the gearbox components, a more common situation is to have stops triggered by the safety supervision of the robot. The safety supervision may be triggered due to the presence of torque levels exceeding a maximum allowed level. This torque limit can thus be used to find the level of w which would cause a robot stop by the safety supervision system.

In order to allow for condition based maintenance, the wear changes should be detected before a failure takes place. In fact, an alarm should be generated early enough so that appropriate maintenance actions can take place with minimal interference, allowing for CBM. Because wear will develop with time depending on how the robot is used, it is difficult to

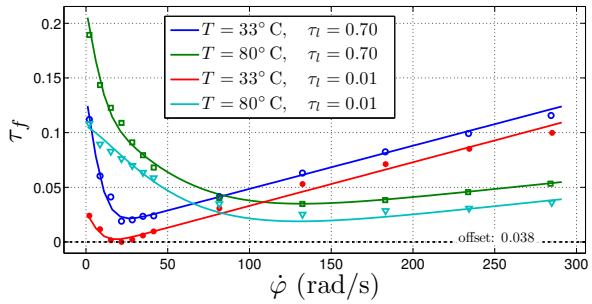

(a) Observed friction curves (circles) and model-based predictions (lines) given by (5) for low and high values of T and τ_l and no significant wear.

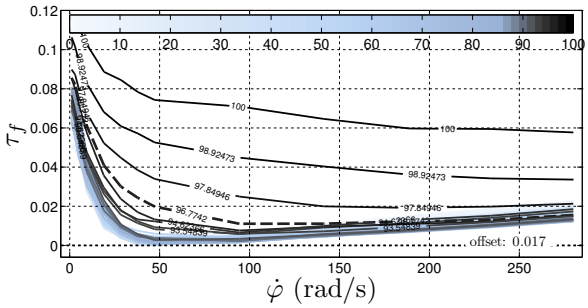

(b) Wear effects from accelerated tests. The colormap is related to the length of the tests with values between 0 and 100. The dashed line relates to a wear level critical for CBM.

Fig. 2. Friction dependencies in a robot joint based on experimental studies. The offset values were removed for a comparison, their values are shown in the dotted lines. The data were collected for similar gearboxes and are presented in directly comparable scales. Notice the larger amplitude of effects caused by temperature and load compared to those caused by wear but the different speed dependence.

TABLE II
PARAMETERS FOR THE MODEL (7) AND ONE STANDARD DEVIATION IDENTIFIED USING THE WEAR PROFILE DATA AT $k = 96.77$ WITH $\mathsf{w} = 35$.

$F_{s,\mathsf{w}}\,[10^{-4}]$	$F_{v,\mathsf{w}}\,[10^{-7}]$	$\dot{\varphi}_{s,\mathsf{w}}$
9.02 ± 0.19	-5.15 ± 1.00	2.19 ± 0.15

determinate a priori a critical wear level to be detected. This can be addressed with the development of lifetime models for prognosis which is outside the scope of this work. Often, lifetime models are developed based on the statistical behavior of failure data [22]. Lifetime models are typically found during product development and require a large number of observations to achieve models which are statistically significant.

1) Identification: The model (7) is identified with the wear profile data of Fig. 3. For these data, a robot stop triggered by the safety supervision occurs at $k = 100$ which is considered as a failure state. Based on a lifetime model developed for this robot, the robot manufacturer decided that in order to allow for CBM, it is critical to detect the wear level at $k = 96.77$. Because it is important that the wear model is most accurate for this critical level, the data collected at $k = 96.77$ are used for the identification of the parameters of the wear model under the convention that $\mathsf{w} = 35$. This convention is adopted because the value of $\widetilde{\tau}_f$ at $k = 96.77$ and $\dot{\varphi} = 28$ rad/s is around 35% of the maximum value of $\widetilde{\tau}_f$ for the entire data, which occurs at $k = 100$ and same speed. The parameter α is fixed to 1.36 for consistency with the parameters found for (5), given in Table I. The identification method described in [17] is used to find the remaining parameters, which are shown in Table II.

2) Validation: Considering the identified parameters for the model in (7), the wear levels of Fig. 3 are identified for each k. With the identified wear values, the wear profile given by model predictions from (7) and observations are presented for the interval $k = [94, 98]$ in Fig. 4. As can be noticed, the model can predict well the behavior of $\widetilde{\tau}_f$. The mean and standard deviation for the prediction error of the wear model in (7), nominated here as $\widetilde{\varepsilon}$, were estimated as $[\mu_{\widetilde{\varepsilon}}, \sigma_{\widetilde{\varepsilon}}] = [9.72\,10^{-4}, 3.82\,10^{-3}]$.

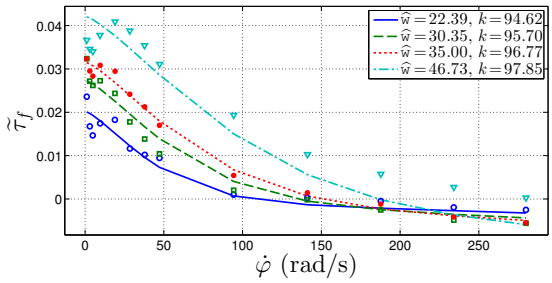

Fig. 4. Observed wear profile data (circles) and model predictions (lines).

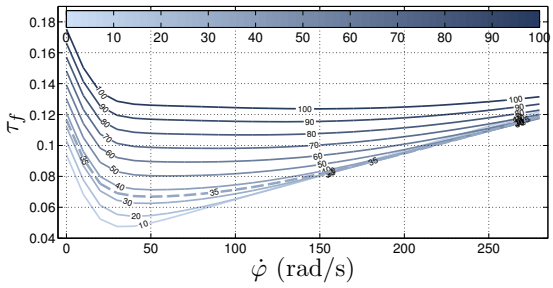

Fig. 5. Increase of wear levels given by the model (8) with colormap indicating w. The dashed line relates to the critical wear level $\mathsf{w} = 35$.

D. A Complete Model of Steady-State Friction

Under the assumption that the effects of load and temperature are independent of those caused by wear, it is possible to extend the model given in (5) to include the effects of wear as

$$\tau_f(\dot{\varphi}, \tau_l, T, \mathsf{w}) = \tau_f^0(\dot{\varphi}, \tau_l, T) + \widetilde{\tau}_f(\dot{\varphi}, \mathsf{w}), \tag{8}$$

where $\tau_f^0(\dot{\varphi}, \tau_l, T)$ is given by (5) and $\widetilde{\tau}_f(\dot{\varphi}, \mathsf{w})$ is described in (7). Fig. 5 presents the friction predictions given by the proposed model at $T = 40°\mathrm{C}$ and $\tau_l = 0.10$ for wear values in the range $\mathsf{w} = [0,\ 100]$ when the parameters given in Tables I and II are used. Notice that the effects are concentrated in the speed range between $0 - 150$ rad/s and also that the resulting friction curves show good resemblance to Fig. 2(b). As previously, the dashed line in Fig. 5 indicates an alarm level for the wear with $\mathsf{w} = 35$.

III. MODEL-BASED WEAR ESTIMATION

Consider that the experiment described in Sec. II-A is repeated N times independently under the same load τ_l and temperature T at speed levels

$$\dot{\Phi} = [\dot{\varphi}^{(1)}, \cdots, \dot{\varphi}^{(i)}, \cdots, \dot{\varphi}^{(N)}]^T$$

generating the related steady-state friction data points

$$\mathcal{T}_f = [\tau_f^{(1)}, \cdots, \tau_f^{(i)}, \cdots, \tau_f^{(N)}]^T.$$

A model for each steady-state friction datum $\tau_f^{(i)}$ can be achieved by including an additive uncertainty term to the model in (8). Assuming that the prediction errors for models (5) and (7) follow independent Gaussian distributions, $\varepsilon \sim \mathcal{N}(\mu_\varepsilon, \sigma_\varepsilon^2)$ and $\widetilde{\varepsilon} \sim \mathcal{N}(\mu_{\widetilde{\varepsilon}}, \sigma_{\widetilde{\varepsilon}}^2)$, the resulting *data generation model* is

$$\begin{aligned} \tau_f^{(i)} &= \tau_f^0(\dot{\varphi}^{(i)}, \tau_l, T) + \varepsilon + \widetilde{\tau}_f(\dot{\varphi}^{(i)}, \mathsf{w}) + \widetilde{\varepsilon} \\ &= \tau_f(\dot{\varphi}^{(i)}, \tau_l, T, \mathsf{w}) + \bar{\varepsilon} \qquad (9a) \end{aligned}$$

$$\bar{\varepsilon} \sim \mathcal{N}(\mu_{\bar{\varepsilon}},\, \sigma_{\bar{\varepsilon}}^2), \quad \mu_{\bar{\varepsilon}} = \mu_\varepsilon + \mu_{\widetilde{\varepsilon}}, \quad \sigma_{\bar{\varepsilon}}^2 = \sigma_\varepsilon^2 + \sigma_{\widetilde{\varepsilon}}^2. \qquad (9b)$$

Considering $\mu_{\bar{\varepsilon}} \approx 0$, the joint density function for $\mathcal{T}_f$ is

$$p(\mathcal{T}_f | \tau_l, T, \mathsf{w}) = \mathcal{N}\left(\mathcal{T}_f; \boldsymbol{\tau_f}(\dot{\Phi}, \tau_l, T, \mathsf{w}), \Sigma\right) \qquad (10)$$

with $\Sigma = I\sigma_{\bar{\varepsilon}}^2$ and

$$\begin{aligned} \boldsymbol{\tau_f}(\dot{\Phi}, \tau_l, T, \mathsf{w}) = [&\tau_f(\dot{\varphi}^{(1)}, \tau_l, T, \mathsf{w}), \cdots, \\ &\tau_f(\dot{\varphi}^{(i)}, \tau_l, T, \mathsf{w}), \cdots, \tau_f(\dot{\varphi}^{(N)}, \tau_l, T, \mathsf{w})]^T \end{aligned}$$

where $\tau_f(\cdot)$ is the nonlinear function given by (8).

An unbiased estimate of the load torque τ_l is considered available, achieved, e.g., using a robot model, with distribution $\mathcal{N}(\tau_l; \mu_{\tau_l}, \sigma_{\tau_l}^2)$. The information from this estimate is included in the model by considering the *marginal density* function

$$\bar{p}(\mathcal{T}_f | T, \mathsf{w}) = \int_{-\infty}^{\infty} p(\mathcal{T}_f | \tau_l, T, \mathsf{w}) \mathcal{N}(\tau_l; \mu_{\tau_l}, \sigma_{\tau_l}^2)\, \mathrm{d}\tau_l \qquad (11)$$

which for the Gaussian distribution $p(\mathcal{T}_f | \tau_l, T, \mathsf{w})$ given in (10) can be found explicitly since the dependence of $\boldsymbol{\tau_f}(\cdot)$ on τ_l is linear, see (5). The marginal density function is given by [23, p. 93]

$$p(\mathcal{T}_f | T, \mathsf{w}) = \mathcal{N}\left(\mathcal{T}_f; \boldsymbol{\tau_f}(\dot{\Phi}, T, \mathsf{w}), \Sigma(\dot{\Phi})\right) \qquad (12)$$

where

$$\begin{aligned} \boldsymbol{\tau_f}(\dot{\Phi}, T, \mathsf{w}) &\triangleq \boldsymbol{\tau_f}(\dot{\Phi}, \mu_{\tau_l}, T, \mathsf{w}) \qquad (13) \\ \Sigma(\dot{\Phi}) &= \Sigma + M(\dot{\Phi}) M(\dot{\Phi})^T \sigma_{\tau_l}^2 \qquad (14) \\ M(\dot{\Phi}) &\triangleq [m(\dot{\varphi}^{(1)}), \cdots, m(\dot{\varphi}^{(i)}), \cdots, m(\dot{\varphi}^{(N)})]^T \\ m(\dot{\varphi}) &\triangleq F_{c,\tau_l} + F_{s,\tau_l} e^{-\left|\frac{\dot{\varphi}}{\dot{\varphi}_{s,\tau_l}}\right|^\alpha}, \end{aligned}$$

notice the clash of notation in (13). It is further considered that the *model parameters are known*.

In this setting, the vector of unknowns is $\theta = [T, \mathsf{w}]^T$ has the log-likelihood function

$$\log \mathcal{L}(\theta) = \log \mathcal{N}\left(\mathcal{T}_f; \boldsymbol{\tau_f}(\dot{\Phi}, \theta), \Sigma(\dot{\Phi})\right). \qquad (15)$$

Based on the achieved likelihood function, Sec. III-A discusses maximum likelihood estimators of w. The estimate is, of course, dependent on $\mathcal{T}_f$ and thus on the choice of $\dot{\Phi}$. For a limited number of friction observations N, the problem of *experiment design* is to choose $\dot{\Phi}$ such that the estimated wear level is as accurate as possible. Experiment design is described in Sec. III-B.

A. Maximum Likelihood Estimation

The *maximum likelihood* estimate of θ given the data vector $\mathcal{T}_f$ is the value for which the log-likelihood function, given in (15), has a maximum, i.e.

$$\widehat{\theta} = \arg\max_\theta \log \mathcal{L}(\theta).$$

The terms dependent on θ in the log-likelihood function have the form

$$\log \mathcal{L}(\theta) \propto -\left[\mathcal{T}_f - \boldsymbol{\tau_f}(\dot{\Phi}, \theta)\right]^T \Sigma(\dot{\Phi})^{-1} \left[\mathcal{T}_f - \boldsymbol{\tau_f}(\dot{\Phi}, \theta)\right],$$

and the problem is therefore a weighted nonlinear least-squares, where T and w are estimated jointly. To restrict the search space, it is possible to add constraints to the problem according to available knowledge of the unknowns. Naturally, $\mathsf{w} \geq 0$, and it is also possible to include lower and upper limits for the temperature, denoted $\underline{T}$ and $\overline{T}$ respectively. For a robot operating in a controlled indoor environment, $\underline{T}$ would be the minimum room temperature while $\overline{T}$ is given by the maximum room temperature and self heating of the joint due to actuator losses. This gives the problem

$$\begin{aligned} [\widehat{T}, \widehat{\mathsf{w}}] = \arg\min_{T,\mathsf{w}} &\left[\mathcal{T}_f - \boldsymbol{\tau_f}(\dot{\Phi}, T, \mathsf{w})\right]^T \Sigma(\dot{\Phi})^{-1} \\ &\left[\mathcal{T}_f - \boldsymbol{\tau_f}(\dot{\Phi}, T, \mathsf{w})\right] \qquad (16) \\ \text{s.t.} \quad &0 \leq \mathsf{w} \\ &\underline{T} \leq T \leq \overline{T}, \end{aligned}$$

which is solved using `lsqnonlin` available in Matlab's Optimization Toolbox with initial values found from a coarse grid search.

The estimator of (16) is valid for $N \geq 2$ since at least two equations are needed to solve for the two unknowns. For $N = 1$, an approximation of the marginalized likelihood function $p(\mathcal{T}_f | \mathsf{w})$ can be used. Considering that T can occur with equal probability over its domain, i.e. $T \sim \mathcal{U}(\underline{T}, \overline{T})$, the marginalized likelihood function is,

$$p(\mathcal{T}_f | \mathsf{w}) = \frac{1}{\overline{T} - \underline{T}} \int_{\underline{T}}^{\overline{T}} p(\mathcal{T}_f | T, \mathsf{w})\, \mathrm{d}T. \qquad (17)$$

Since there is no analytical solution for (17), Monte Carlo Integration (MCI) is used to approximate it in a symbolic expression in w as

$$\widehat{p}(\mathcal{T}_f | \mathsf{w}) = \frac{1}{N_T} \sum_{i=1}^{N_T} p(\mathcal{T}_f |, T^{(i)}, \mathsf{w}) \qquad (18)$$

for N_T randomly generated samples $T^{(i)} \sim \mathcal{U}(\underline{T}, \overline{T})$.

Using the approximated marginalized likelihood function of (18) leads to the problem

$$\begin{aligned} \widehat{\mathsf{w}} &= \arg\min_{\mathsf{w}} \; -\widehat{p}(\mathcal{T}_f|\mathsf{w}) \\ &\text{s.t.} \quad 0 \leq \mathsf{w}. \end{aligned} \tag{19}$$

This nonlinear constrained minimization is solved using `fmincon` from the Optimization Toolbox in Matlab with initial values taken from a coarse grid search.

B. Experiment Design

An estimate $\widehat{\theta}$ of θ is dependent on the data $\mathcal{T}_f$, the associated $\dot{\Phi}$ and on the estimator used. The mean square error of an estimate can be used as a criterion to assess how the choice of $\dot{\Phi}$ affects the performance. Let the bias of an estimate $\widehat{\theta}$ be denoted $b(\theta) \triangleq \mathbb{E}[\widehat{\theta}] - \theta$, then from the Cramér-Rao lower bound (see e.g. [24, Exercise 2.4.17]), it follows

$$\begin{aligned} &\mathrm{MSE}(\widehat{\theta}) = \mathbb{E}\left[(\widehat{\theta} - \theta)^2\right] = \mathrm{Var}(\widehat{\theta}) + b(\theta) b^T(\theta) \\ &\geq b(\theta) b(\theta)^T + \left[I + \nabla_\theta b(\theta)\right] F(\theta)^{-1} \left[I + \nabla_\theta b(\theta)\right]^T \end{aligned} \tag{20}$$

where

$$F(\theta) = \mathbb{E}\left[\nabla_\theta \log \mathcal{L}(\theta) (\nabla_\theta \log \mathcal{L}(\theta))^T\right] \tag{21}$$

is the Fisher information matrix. Neglecting the bias term, which is a function of the estimator used, $\mathrm{MSE}(\widehat{\theta}) \geq F(\theta)^{-1}$. The achieved bound can be minimized by affecting the inverse of the Fisher information matrix, improving the achievable performance for any unbiased estimator. For the log-likelihood function in (15), the Fisher information matrix is given by (see [25] for a proof)

$$F(\dot{\Phi}, \theta) = [\nabla_\theta \boldsymbol{\tau_f}(\dot{\Phi}, \theta)] \Sigma(\dot{\Phi})^{-1} [\nabla_\theta \boldsymbol{\tau_f}(\dot{\Phi}, \theta)]^T \tag{22}$$

where the dependence on $\dot{\Phi}$ is highlighted.

The objective of the experiment design is to choose $\dot{\Phi}$ that minimizes the bound on $\widehat{\mathsf{w}}$, i.e. $\mathrm{MSE}(\widehat{\mathsf{w}})$. For $\theta = [T, \mathsf{w}]^T$, $\mathrm{MSE}(\widehat{\mathsf{w}})$ corresponds to the 2,2-element of the inverse of the information matrix and the problem is thus

$$\dot{\Phi}^* = \arg\min_{\dot{\Phi}} \; [F(\dot{\Phi}, \theta)^{-1}]_{2,2}, \tag{23}$$

where $[\cdot]_{i,j}$ denotes the i,j-element of a matrix. Dropping the argument for $F(\dot{\Phi}, \theta)$, the analytical expression for $[F^{-1}]_{2,2}$ is given by

$$[F^{-1}]_{2,2} = \frac{[F]_{1,1}}{[F]_{1,1}[F]_{2,2} - [F]_{1,2}^2}.$$

For a positive definite $\Sigma(\dot{\Phi})$, the problem is well-posed only if $\nabla_\theta \boldsymbol{\tau_f}(\dot{\Phi}, \theta)$ has rank equal to the number of unknowns. This can only be achieved if $N \geq 2$ and if there are at least two linear independent columns in $\nabla_\theta \boldsymbol{\tau_f}(\dot{\Phi}, \theta)$, e.g. if at least two different speed values are chosen. To ensure the later, additional constraints are added to keep a minimum separation, $\delta_{\dot{\varphi}}$, between each speed level in $\dot{\Phi}$. Furthermore, the search is limited to the minimum $\underline{\dot{\varphi}}$ and maximum $\overline{\dot{\varphi}}$ speed levels for which the experiment of Sec. II-A can be performed. The optimal speed values are therefore given as the solution to the problem

$$\begin{aligned} \dot{\Phi}^* &= \arg\min_{\dot{\Phi}} \; [F(\dot{\Phi}, \theta)^{-1}]_{2,2} \\ &\text{s.t.} \quad \dot{\varphi}^{(i)} - \dot{\varphi}^{(j)} \leq -\delta_{\dot{\varphi}}, \; (i < j) \\ &\qquad \underline{\dot{\varphi}} \leq \dot{\varphi}^{(i)} \leq \overline{\dot{\varphi}} \end{aligned} \tag{24}$$

This is a constrained nonlinear minimization which is solved here using `fmincon` in Matlab with initial values found from a coarse grid search.

The case where $N = 1$ can be considered by using the approximated marginalized likelihood function given by (18). Using this approximation the Fisher information matrix is

$$F(\dot{\Phi}, \mathsf{w}) \triangleq \mathbb{E}\left[\left(\frac{\partial \log \widehat{p}(\mathcal{T}_f|\mathsf{w})}{\partial \mathsf{w}}\right)^2\right].$$

The differentiation of $\widehat{p}(\cdot)$ is performed symbolically and the expectation is computed using MCI with N_{τ_f} samples taken from $\widehat{p}(\mathcal{T}_f|\mathsf{w})$ in (18), leading to the estimate $\widehat{F}(\dot{\Phi}, \mathsf{w})$ of $F(\dot{\Phi}, \mathsf{w})$. The associated optimization problem is thus

$$\begin{aligned} \dot{\Phi}^* &= \arg\min_{\dot{\Phi}} \; \widehat{F}(\dot{\Phi}, \mathsf{w})^{-1} \\ &\text{s.t.} \quad \underline{\dot{\varphi}} \leq \dot{\varphi}^{(i)} \leq \overline{\dot{\varphi}} \end{aligned} \tag{25}$$

which is also a constrained nonlinear minimization problem and is solved in the same manner as (24).

IV. SIMULATION STUDY

A simulation study is first considered to illustrate the use of the experiment design criteria defined in Sec. III-B and wear estimators proposed in Sec. III-A.

A. Definition of Parameters Used

The framework of Sec. III requires knowledge of the friction model parameters in the data generation model (9). The parameters for the nominal part given in (5) can be identified for a new robot using joint temperature measurements and an estimate of the joint load torques, see e.g. [17]. The parameters for (7), describing the wear behavior, are more difficult because failure data are required. For CBM, wear estimates are needed before a failure of the system, in which case the parameters for (7) cannot be known in advance. This can however be overcome with the use of historical failure data. The simulation studies that follows illustrate the case where these models are known, focusing on the effects of temperature and load uncertainties. In Sec. V, the effects of uncertainties in the wear model are studied based on real data.

Here, the friction parameters used are given in Tables I and II which were identified for joint 2 of an ABB IRB 6620 industrial robot. The noise properties of (9b) are taken from the model validation in Secs. II-B1 and II-C2. Applying (9b) to these values gives $\mu_{\bar{\varepsilon}} = 4.80\,10^{-5} \approx 0$ and $\sigma_{\bar{\varepsilon}} = 5.70\,10^{-3}$. The mean and standard deviation for the load estimate used in (11) are chosen as $\mu_{\tau_l} = 0.5$ and $\sigma_{\tau_l} = 0.1$. Finally, The optimization parameters used in the identification and experiment design problems are given in Table III.

TABLE III
OPTIMIZATION PARAMETERS.

Experiment design			Identification		Approximations	
$\underline{\dot{\varphi}}$	$\overline{\dot{\varphi}}$	$\delta_{\dot{\varphi}}$	$\underline{T}$	$\overline{T}$	N_T	N_{τ_f}
1	280	5	30	50	100	200

TABLE IV
CHOICE OF OPTIMAL SPEED VALUES FOR DIFFERENT VALUES OF N. "COST" IS THE VALUE OF THE OBJECTIVE FUNCTION IN (25) ($N=1$) OR (24) ($N \geq 2$) COMPUTED AT $\dot{\Phi}^*$.

N	Cost	$\dot{\Phi}^*$
1	45.91	33.78
2	26.01	$[35.84, 40.84]^T$
3	19.65	$[33.68, 38.68, 43.68]^T$
4	16.50	$[31.65, 36.65, 41.65, 46.65]^T$

B. Experiment Design

As discussed in Sec. III, the objective of experiment design is to choose $\dot{\Phi}$ that gives as high accuracy as possible for the wear estimate. From a practical perspective, it is also important to limit the number of friction data points N. Here, the experiment design will be considered for $N=[1,2,3,4]$. For friction data collected according to the experiment defined in Sec. II-A, this would thus give up to one minute of total experimentation time for a six axis robot.

The problems (25) and (24) are solved for $N=1$ and $N=[2,3,4]$ respectively when $[T,\mathsf{w}]=[40,35]$. The optimal speed values found are shown in Table IV, which have values in a region between $30-50$ rad/s.

To provide more insights of the experiment design problem, note that the information matrix used in the optimal solution for (24) is dependent on products of the terms

$$f'_T(T,\dot{\varphi}) \triangleq \frac{\partial \tau_f(\dot{\varphi},\theta)}{\partial T}, \quad f'_{\mathsf{w}}(\mathsf{w},\dot{\varphi}) \triangleq \frac{\partial \tau_f(\dot{\varphi},\theta)}{\partial \mathsf{w}} \qquad (26)$$

which, because of the model structure, are function only of $\dot{\varphi}$ and the differentiation variable. These derivatives relate to the information about T and w contained in the model. A large absolute value of these derivatives corresponds to more information about the particular parameter. The aim of the experiment design is to gather information about w, and hence it is natural that speed points are selected where $|f'_{\mathsf{w}}|$ is larger than $|f'_T|$ as it is possible. The terms $|f'_{\mathsf{w}}|$ and $|f'_T|$ evaluated at $[T,\mathsf{w}]=[40,35]$ are shown in Fig. 6(a) as a function of $\dot{\varphi}$. For the speed region of $30-50$ rad/s, it is possible to note that $|f'_{\mathsf{w}}|$ is larger than $|f'_T|$ by a factor of two.

The model gradients are however dependent on the operating point for T and w. Therefore, it is not possible to select $\dot{\Phi}$ that is optimal in general. To illustrate these dependencies, Fig. 7 shows contour plots of $|f'_{\mathsf{w}}|$ and $|f'_T|$ as a function of speed, T and w. The dashed lines in Fig. 7 relate to the value where the derivatives are zero. In both sub figures, the gradients have negative values to the right of the dashed lines and are otherwise positive. Unfortunately, $|f'_T|$ is often larger than $|f'_{\mathsf{w}}|$ (notice that the scale used for f'_T is a factor of ten times larger than for f'_{w}). Nevertheless, the different speed dependencies allow for a selective choice of $\dot{\Phi}$ that improves performance of the wear estimates.

To illustrate how the optimal speed region can vary with operating points, Fig. 6(b) displays the speed region where $|f'_{\mathsf{w}}| > 2|f'_T|$ when $\mathsf{w}=35$, i.e. the critical value to be detected, and T varies in the range $30-50$ C°. Notice that this speed region is not optimal in the sense of (24) or (25), but relates to a region where the information for w is considerably larger than for T. As it can be seen, only a narrow band of speed values contain useful information for the estimation of w for a particular value of T. The speed band also varies with temperature, with no overlap over all temperature values considered.

It is important to emphasize that the characteristics shown here are valid for the specific model parameters used and different properties are expected for different robots and gearboxes. A similar behavior of temperature and wear have however been observed for various robot units equipped with a similar type of gearbox. Furthermore, different criteria than (23) could be used. The criterion used here has the purpose to achieve as accurate as possible estimate $\widehat{\mathsf{w}}$, irrespective of the performance for $\widehat{T}$. A different criterion could be, e.g. to minimize the trace of $F(\dot{\Phi},\theta)^{-1}$, which would choose $\dot{\Phi}$ with a different relevance to the effects of T.

C. Bias and Variance Properties of the Wear Estimators

With the optimal speed values found in Table IV, the bias and variance properties of the proposed estimators are evaluated based on Monte Carlo simulations. The true wear level is fixed at $\mathsf{w}=35$ and temperature is varied in the range $T=[30,50]$. The data generated by (9) are input to (19) or (16) for $N=1$ and $N=[2,3,4]$ respectively, and the estimation is repeated a total of $N_{\mathrm{MC}}=1\,10^3$ times per operating point.

Fig. 8 shows the simulation results for the bias and variance of the estimators as a function of the true temperature level T. As it can be seen, the bias and variance are reduced with N. The reduction in the variance is specially large for $N=2$ compared to $N=1$, which is related to marginalization effects of T. The bias presents a nonlinear behavior with T while the variance seems to be unaffected by T.

V. STUDIES BASED ON REAL DATA

Gathering enough informative data related to wear from the field would have been inviable since wear faults take a long time to develop and are infrequent. Even in accelerated wear tests, it may take several months or years before wear effects become significant. Another difficulty with such tests is the high cost of running several robots to obtain reliable statistics. Moreover, temperature studies are challenging since the thermal constant of a large robot is of several hours.

Other than simulation studies, the only viable alternative in the research project was to combine nominal friction data (with no acute wear present) and wear profile data, collected from a different robot of the same type from accelerated wear tests under constant load and temperature conditions. The nominal and wear profile datasets are denoted $\boldsymbol{\mathcal{T}_f}^0$ and $\widetilde{\boldsymbol{\mathcal{T}}}_{\boldsymbol{f}}$ respectively. These data were collected from axis 2 of an ABB IRB 6620 industrial robot, equipped with a rotary vector gearbox type. Each of these datasets are matrices where each row contains

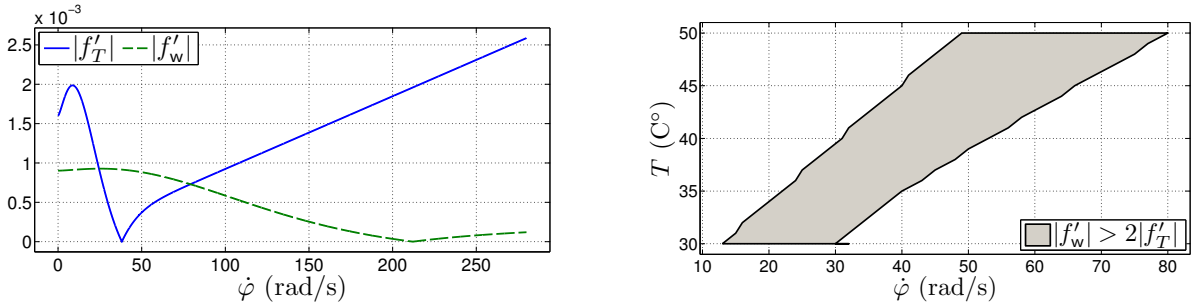

(a) $|f'_T|$ and $|f'_{\mathsf{w}}|$. (b) Speed region where $|f'_{\mathsf{w}}| > 2|f'_T|$.

Fig. 6. (a) Behavior of f'_{w} and f'_T with respect to speed evaluated at $[T, \mathsf{w}] = [40, 35]$. (b) The speed regions which give $|f'_{\mathsf{w}}| > 2|f'_T|$ when $\mathsf{w} = 35$ and T varies in the band $[30 - 50]\mathrm{C}^\circ$.

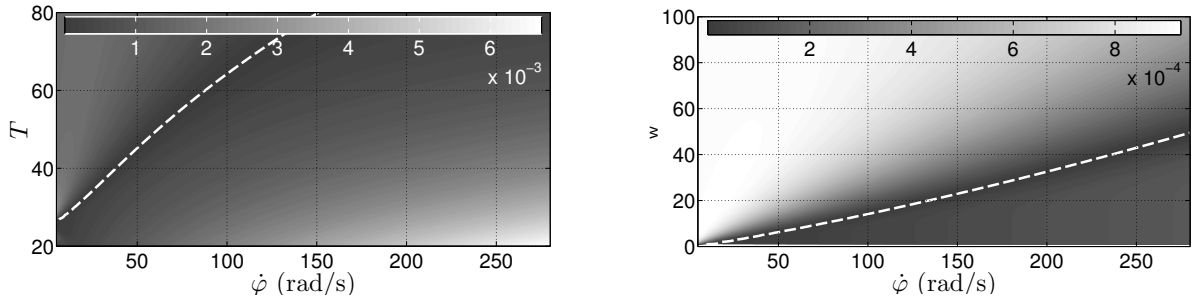

(a) Contour of $|f'_T|$. (b) Contour of $|f'_{\mathsf{w}}|$.

Fig. 7. Absolute value of the friction model gradient for T and w as a function of $\dot{\varphi}$ and differentiation point. Notice that the scale used for f'_T is ten times larger than the scale used for f'_{w}.

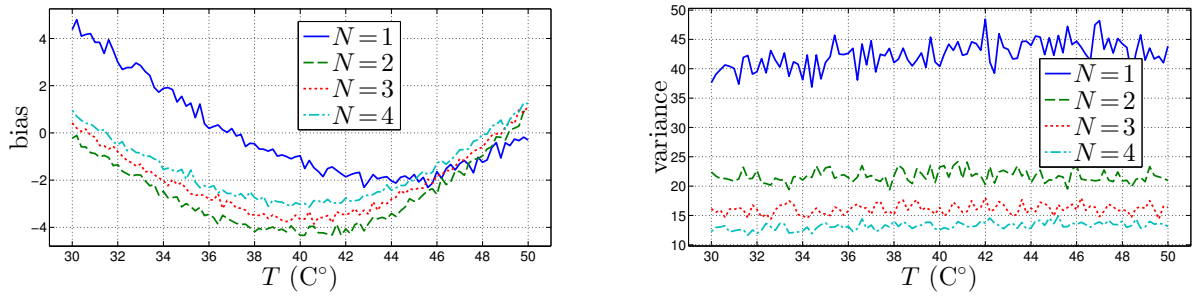

(a) Bias $\mathbb{E}\,[\widehat{\mathsf{w}} - \mathsf{w}]$. (b) Variance $\mathbb{E}\left[(\widehat{\mathsf{w}} - \mathbb{E}\,[\widehat{\mathsf{w}}])^2\right]$.

Fig. 8. Monte Carlo based estimates of bias (a) and variance (b) of the estimators (19) and (16) ($N = 1$ and $N = [2, 3, 4]$ respectively) evaluated with $\mathsf{w} = 35$ and T in the band $30 - 50$ C°.

data from a friction curve collected in the following velocity values

$$\dot{\Phi} = [2.1,\ 8.7,\ 15.3,\ 21.9,\ 28.5,\ 35.1, 41.7,\ 82.2,\ 133.5,\ 184.7,\ 236.2,\ 287.1], \tag{27}$$

i.e., a total of 12 different speed values are possible from these datasets. The nominal dataset, $\boldsymbol{\mathcal{T}_f}^0$, contains data collected under different load and temperature conditions, which are stored in matrices of same size, denoted respectively as $\boldsymbol{\mathcal{T}_l}$ and $\mathbf{T}$. The wear profile data matrix, $\widetilde{\boldsymbol{\mathcal{T}}}_{\boldsymbol{f}}$, has rows associated to the experimentation index k.

The wear profile dataset determines the behavior of friction as a function of k. For a given wear profile dataset, the objective is to emulate friction data collected under varying conditions of load and temperature. First, the desired load and temperature behaviors are pre-defined as a function of k according to $T(k) \in \mathbf{T}$ and $\tau_l(k) \in \boldsymbol{\mathcal{T}_l}$. Second, the datasets are combined as a function of k and the desired speed $\dot{\varphi} \in \dot{\Phi}$, according to

$$\tau_f(k, \dot{\varphi}) = [\boldsymbol{\mathcal{T}_f}^0]_{i_k, j_{\dot{\varphi}}} + [\widetilde{\boldsymbol{\mathcal{T}}}_{\boldsymbol{f}}]_{k, j_{\dot{\varphi}}} \tag{28a}$$

$$j_{\dot{\varphi}} \triangleq \{j : [\dot{\Phi}]_j = \dot{\varphi}\}, \tag{28b}$$

$$i_k \triangleq \{i : [\mathbf{T}]_{i, j_{\dot{\varphi}}} = T(k) \text{ and } [\boldsymbol{\mathcal{T}_l}]_{i, j_{\dot{\varphi}}} = \tau_l(k)\}. \tag{28c}$$

Notice that these data are not analytically generated, but actually based on constant-speed friction data, collected with the experiment described in Sec. II-A. Furthermore, the combination of data according to (28a) is consistent to the model structure in (8) and with the assumption that the effects of wear are independent of those caused by load and temperature.

A. Description of Scenarios

Three different wear profile datasets are considered, they are assigned as $\widetilde{\boldsymbol{\mathcal{T}_f}}^0$, $\widetilde{\boldsymbol{\mathcal{T}_f}}^1$ and $\widetilde{\boldsymbol{\mathcal{T}_f}}^2$. The dataset $\widetilde{\boldsymbol{\mathcal{T}_f}}^0$ was used for the wear modeling presented in Sec. II-C, and is shown in Fig. 3. The other two are shown in Fig. 9. Some relevant characteristics of these datasets are listed below.

- $\widetilde{\boldsymbol{\mathcal{T}_f}}^0$ small random variations, remaining around 0 up to $k = 90$ followed by an exponential increase thereafter.
- $\widetilde{\boldsymbol{\mathcal{T}_f}}^1$ medium random variations, remaining around 0 up to $k = 70$ followed by large increases. It has a maximum amplitude which is 56% of that found in $\widetilde{\mathcal{T}}_f^0$.
- $\widetilde{\boldsymbol{\mathcal{T}_f}}^2$ small random variations, remaining stationary up to $k = 30$ followed by small increases up to $k = 97$ from where it increases steeply. It has a maximum amplitude which is 106% of that found in $\widetilde{\boldsymbol{\mathcal{T}_f}}^0$.

Only one dataset is used to describe the normal behavior of friction and is assigned as $\boldsymbol{\mathcal{T}_f}^0$. Three scenarios are considered using the dataset pairs $(\boldsymbol{\mathcal{T}_f}^0, \widetilde{\boldsymbol{\mathcal{T}_f}}^0)$, $(\boldsymbol{\mathcal{T}_f}^0, \widetilde{\boldsymbol{\mathcal{T}_f}}^1)$ and $(\boldsymbol{\mathcal{T}_f}^0, \widetilde{\boldsymbol{\mathcal{T}_f}}^2)$. The scenarios are called 0, 1 or 2 according to the selected dataset for the wear profile.

To simplify the presentation of the results, the behavior of $T(k)$ and $\tau_l(k)$ are the same for the three scenarios, they are shown in Fig. 10. Notice that the amplitude of the friction changes due to temperature and load are considerably larger than of those caused by wear for any of the scenarios. The maximum change value found for the nominal friction behavior is 157% relative to the maximum change found in $\widetilde{\boldsymbol{\mathcal{T}_f}}^0$.

The same model and optimization parameters considered in Sec. IV-A are used for all scenarios. The parameters for the friction model were identified based on the datasets $\boldsymbol{\mathcal{T}_f}^0$ and $\widetilde{\boldsymbol{\mathcal{T}_f}}^0$. Since these parameters are used for all scenarios, it can be considered that the parameters for the nominal behavior of friction are correct for all scenarios, illustrating the situation where they are found based on experiments performed prior to the tests and when the joint is healthy. The wear parameters are however only consistent for Scenario 0 and Scenarios 1 and 2 illustrate the situation where the wear parameters are based on historical failure data.

B. Results and Discussion

The choice of speed values for experiment design is limited to the speed levels available from the datasets, given in (27). The problems (24) and (25) are solved by considering every possible combination of speed levels for $N = [1, 2, 3, 4]$. The resulting optimal values are given in Table V and relate well to those found in Table IV. Notice that the optimal values depend on the wear model parameters used. Since these parameters were found using $\widetilde{\boldsymbol{\mathcal{T}_f}}^0$, optimality of $\dot{\Phi}^*$ is only expected for Scenario 0.

The resulting wear estimates for the different scenarios are shown in Figs. 11(a) to 11(c). The same scale for the axes is used in the figures so they are directly comparable. The shaded areas in the figures highlight a region which should be easily distinguishable from the rest in order to allow for an early detection of excessive wear. Noticeably, the wear estimates are consistent to the wear profile data used in all scenarios, even for Scenarios 1 and 2 when the wear model is uncertain. The wear estimates achieved at $k = 100$ for all scenarios show good correspondence to the maximum amplitude change found in the respective wear profile data relative to that found in $\widetilde{\mathcal{T}}_f^0$, for which the wear parameters were found. These observations indicate positively to the viability of the determination of the wear related parameters based on historical data.

TABLE V
CHOICE OF OPTIMAL SPEED VALUES FOR DIFFERENT VALUES OF FRICTION OBSERVATIONS N.

N	Cost	$\dot{\Phi}^*$
1	46.58	35.1
2	26.20	$[35.1, 41.7]^T$
3	22.60	$[28.5, 41.7, 82.2]^T$
4	18.00	$[2.1, 28.5, 35.1, 41.7]^T$

The wear estimates become smoother for larger N, which is in line with the simulation study of Sec. III-A. For all scenarios, the larger wear estimates for $k > 90$ allows for a distinction of the critical (shaded) regions. The detection of a critical wear change could be easily achieved in Scenarios 0 and 1 with a simple threshold, set e.g. at 35. The same threshold would however give an early detection for Scenario 2. An early detection is understood as less critical than a total failure of the system but may lead to unnecessary maintenance actions. More careful analyses of the wear estimates may therefore be needed in order to give an accurate support for maintenance decisions.

The fact that the wear estimates do not differ much with N might lead to the conclusion that $N = 1$ should be used, but this is only true if the optimal speed values are chosen. To illustrate this, two wear estimates were achieved for Scenario 2 using one measurement only, at $\dot{\varphi} = 82.2$ and $\dot{\varphi} = 133.5$. As it can be noticed, the wear estimates are considerably affected by changes in temperature when these speed values are used. However, when these two measurements are used together, the estimate becomes less sensitive. The inclusion of measurements around the optimal speed values should also increase robustness to uncertainties in the wear model.

VI. CONCLUSIONS AND FUTURE WORK

A model-based maximum likelihood wear estimator was proposed based on a known friction model and constant-speed friction data collected from experiments. Because friction is considerably affected by other factors than wear, in particular temperature, a friction model that can describe these variables was suggested. Experiment design was also considered to support the choice of speed levels of the friction data which reveals more information about wear. Simulations and case studies based on real data were considered to evaluate the approach. The wear estimates achieved in the studies showed a clear response to changes of friction, indicating that the approach may open up for condition based maintenance of industrial robots.

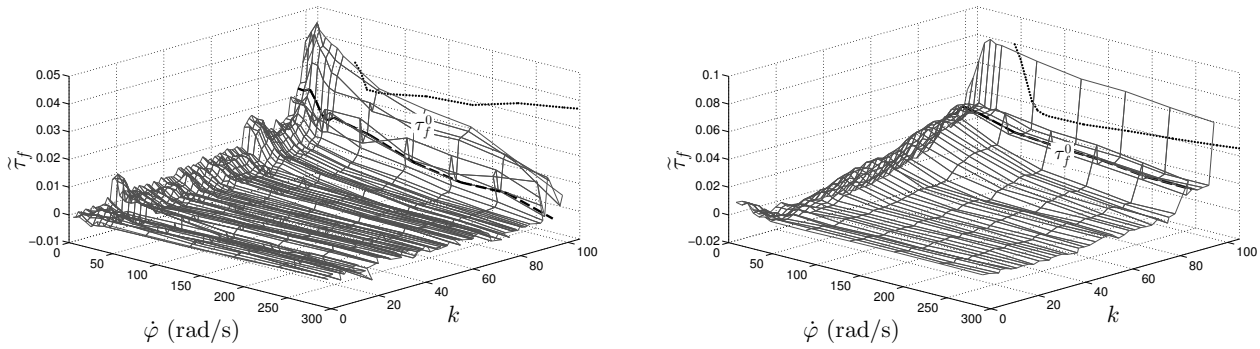

(a) Wear profile data $\widetilde{\boldsymbol{\mathcal{T}}_{\boldsymbol{f}}}^{1}$.

(b) Wear profile data $\widetilde{\boldsymbol{\mathcal{T}}_{\boldsymbol{f}}}^{2}$.

Fig. 9. Friction wear profile data used in Scenarios 1 (a) and 2 (b). The dashed line indicates a critical wear level to be found. The dotted lines relate to the nominal (wear free) friction curve τ_f^0 that was removed from the friction data according to (6).

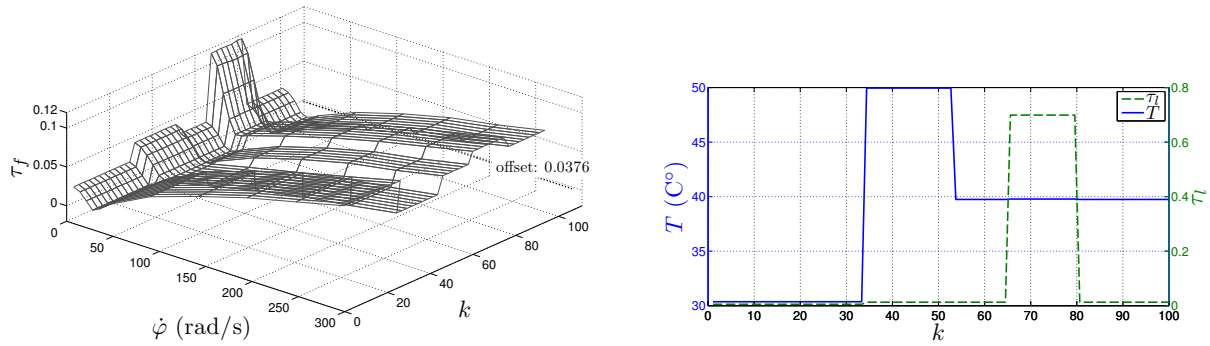

(a) Nominal friction behavior for all scenarios.

(b) Associated T and τ_l.

Fig. 10. Behavior of nominal friction as a function of $\dot{\varphi}$ and k for the scenarios considered (a); an offset value corresponding to the smallest friction value in the dataset was removed for a comparison to the wear effects. The associated temperature and load values are shown in (b).

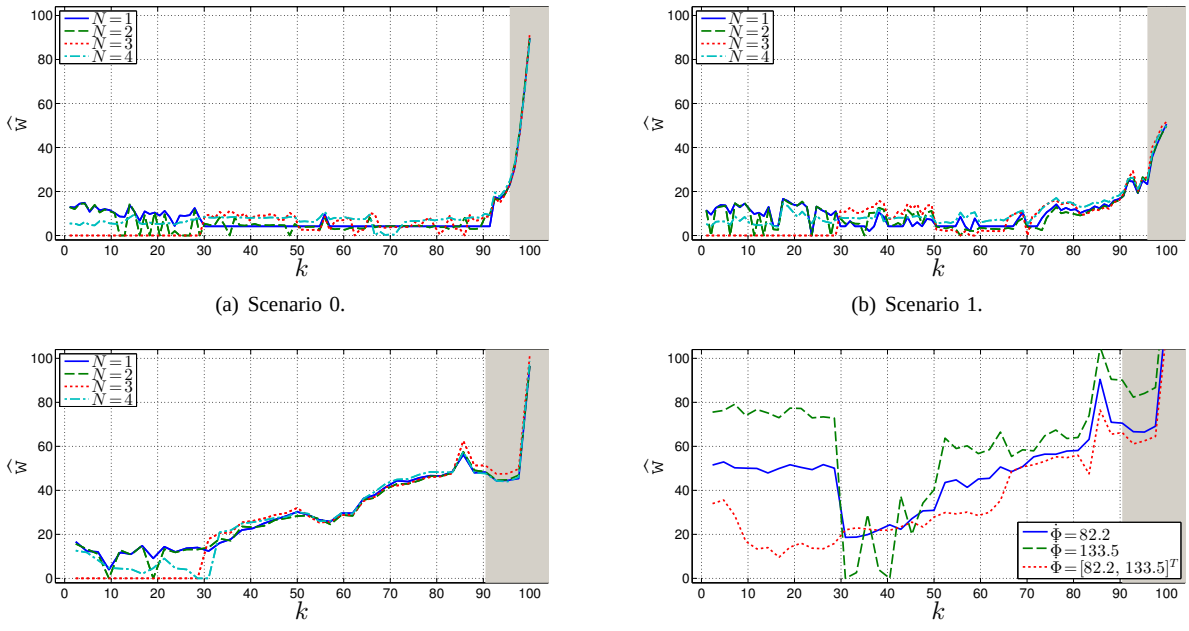

(a) Scenario 0.

(b) Scenario 1.

(c) Scenario 2.

(d) Scenario 2 with non-optimal speed values.

Fig. 11. Wear estimates for the different scenarios investigated. Figs. (a) to (c) present the estimates for $N=[1,2,3,4]$ using the optimal speed values. Fig. (d) illustrates Scenario 2 when non-optimal speed values are used for $N=[1,2]$. The shaded areas in the figures relate to a region where a detection should be made.

The studies presented here are restricted to one type of robot/gearbox and in an experimental verification performed in a lab. To verify the applicability of the proposed solutions in an industrial scenario, a more extensive experimental campaign is needed. Also interesting is to consider other types of variations and how these affect the models and framework presented. For example, a change of lubricant may require the re-estimation of all or some of the friction parameters used.

It should be stressed that different characteristics of the problem are expected for different devices, gearboxes and fault mechanisms. The results and discussion presented here can however provide useful guidance for those interested in using similar approaches for different devices. Of key importance to the proposed approach are the friction models used. The same ideas suggested for experiment design and wear identification can nevertheless be extended to other devices and model structures as long as the friction model used is a static function of wear. These problems can be addressed with the resulting likelihood function. In case there are at least as many friction data points as unknowns, the standard joint likelihood function can be used, otherwise the marginalized likelihood is a suitable alternative.

A natural extension to this work is to consider on-line wear estimation. This could perhaps be achieved by considering data from a friction observer, e.g. as presented in [11], [16]. The sensitivity of such approach to unmodeled phenomena, e.g. due to dynamic friction, and external disturbances should be considered carefully based on experiments performed on a real robot in different scenarios.

REFERENCES

[1] A. R. Lansdown, A. L. Price, and J. Larsen-Basse, "Materials to resist wear—a guide to their selection and use," *Journal of Tribology*, vol. 109, no. 2, pp. 379–380, 1987.

[2] J. A. Williams, "Wear and wear particles - some fundamentals," *Tribology International*, vol. 38, no. 10, pp. 863 – 870, 2005.

[3] K. Kato, "Wear in relation to friction – a review," *Wear*, vol. 241, no. 2, pp. 151 – 157, 2000.

[4] A. C. Bittencourt, P. Axelsson, Y. Jung, and T. Brogårdh, "Modeling and identification of wear in a robot joint under temperature disturbances," in *Proc. of the 18th IFAC World Congress*, Milan, Italy, Aug 2011.

[5] V. Filaretov, M. Vukobratovic, and A. Zhirabok, "Observer-based fault diagnosis in manipulation robots," *Mechatronics*, vol. 9, no. 8, pp. 929 – 939, 1999.

[6] M. McIntyre, W. Dixon, D. Dawson, and I. Walker, "Fault identification for robot manipulators," *IEEE Transactions on Robotics*, vol. 21, no. 5, pp. 1028–1034, Oct. 2005.

[7] A. T. Vemuri and M. M. Polycarpou, "A methodology for fault diagnosis in robotic systems using neural networks," *Robotica*, vol. 22, no. 04, pp. 419–438, 2004.

[8] W. E. Dixon, I. D. Walker, D. M. Dawson, and J. P. Hartranft, "Fault detection for robot manipulators with parametric uncertainty: A prediction-error-based approach," *IEEE Transactions on Robotics and Automation*, vol. 16, no. 6, pp. 3628–3634, 2000.

[9] F. Caccavale, P. Cilibrizzi, F. Pierri, and L. Villani, "Actuators fault diagnosis for robot manipulators with uncertain model," *Control Engineering Practice*, vol. 17, no. 1, pp. 146 – 157, 2009.

[10] A. De Luca and R. Mattone, "Actuator failure detection and isolation using generalized momenta," in *Proc. of the 2003 IEEE International Conference on Robotics and Automation (ICRA)*, vol. 1, Taipei, Taiwan, sept. 2003, pp. 634 – 639 vol.1.

[11] L. R. Ray, J. R. Townsend, and A. Ramasubramanian, "Optimal filtering and Bayesian detection for friction-based diagnostics in machines," *ISA Transactions*, vol. 40, no. 3, pp. 207 – 221, 2001.

[12] W. Chen, "Fault detection and isolation in nonlinear systems: observer and energy-balance based approaches," Dissertation, Faculty of Eng. Automatic Control and Complex Systems, Duisubug-Essen University, Oct 2011.

[13] L. Marton, "Energetic approach to deal with faults in robot actuators," in *Proc. of the 20th Mediterranean Conference on Control Automation (MED)*, Barcelona, Spain, july 2012, pp. 85 –90.

[14] B. Freyermuth, "An approach to model based fault diagnosis of industrial robots," in *Proc. of the 1991 IEEE International Conference on Robotics and Automation (ICRA)*, vol. 2, Sacramento, USA, Apr 1991, pp. 1350–1356.

[15] L. Marton and F. van der Linden, "Temperature dependent friction estimation: Application to lubricant health monitoring," *Mechatronics*, vol. 22, no. 8, pp. 1078 – 1084, 2012.

[16] L. Marton, "On-line lubricant health monitoring in robot actuators," in *Proc. of the 2011 Australian Control Conference (AUCC)*, Melbourne, Australia, nov. 2011, pp. 167 –172.

[17] A. C. Bittencourt and S. Gunnarsson, "Static friction in a robot joint—modeling and identification of load and temperature effects," *Journal of Dynamic Systems, Measurement, and Control*, vol. 134, no. 5, 2012.

[18] F. Al-Bender and J. Swevers, "Characterization of friction force dynamics," *IEEE Control Systems Magazine*, vol. 28, no. 6, pp. 64–81, 2008.

[19] K. De Moerlooze, F. Al-Bender, and H. Van Brussel, "A generalised asperity-based friction model," *Tribology Letters*, vol. 40, pp. 113–130, 2010.

[20] P. Hamon, M. Gautier, and P. Garrec, "Dynamic identification of robots with a dry friction model depending on load and velocity," in *Proc. of the 2010 IEEE/RSJ International Conference on Intelligent Robots and Systems*, oct. 2010, pp. 6187 –6193.

[21] N. Kammerer and P. Garrec, "Dry friction modeling in dynamic identification for robot manipulators: Theory and experiments," in *Proc. of the 2013 IEEE International Conference on Mechatronics*, 2013, pp. 422–429.

[22] S. E. Chick and M. B. Mendel, "An engineering basis for statistical lifetime models with an application to tribology," *Reliability, IEEE Transactions on*, vol. 45, no. 2, pp. 208–215, 1996.

[23] C. M. Bishop, *Pattern Recognition and Machine Learning*, 1st ed. New York, USA: Springer, 2006.

[24] H. L. Van Trees, *Detection, Estimation and Modulation Theory, Part I*. Wiley, New York, 2001.

[25] B. Porat and B. Friedlander, "Computation of the exact information matrix of Gaussian time series with stationary random components," *IEEE Transactions on Acoustics, Speech and Signal Processing*, vol. 34, no. 1, pp. 118 – 130, feb 1986.

André Carvalho Bittencourt graduated in Automatic Control Engineer with honors from the Federal University of Santa Catarina, Florianópolis, Brazil. He received a Licentiate degree in January 2012 from Linköping University, Sweden, where he is currently a Ph.D. student. His main research interests are industrial robotics, diagnosis and condition monitoring.

Patrik Axelsson received the M.Sc. degree in applied physics and electrical engineering in January 2009 and the Licentiate degree in automatic control in December 2011, both from Linköping University, Sweden, where he is currently a PhD student. His research interests are sensor fusion and control for industrial manipulators.